High-Power, Kilojoule Class Laser Channeling in Millimeter-Scale Underdense Plasma

L. Willingale,[1] P. M. Nilson,[2] A. G. R. Thomas,[1] J. Cobble,[3] R. S. Craxton,[2] A. Maksimchuk,[1] P. A. Norreys,[4]
T. C. Sangster,[2] R. H. H. Scott,[4] C. Stoeckl,[2] C. Zulick,[1] and K. Krushelnick[1]

[1]*Center for Ultrafast Optical Science, University of Michigan, 2200 Bonisteel Boulevard, Ann Arbor, Michigan 48109, USA*
[2]*University of Rochester-Laboratory for Laser Energetics, Rochester, New York 14623, USA*
[3]*Los Alamos National Laboratory, Los Alamos, New Mexico 87545, USA*
[4]*STFC, Rutherford Appleton Laboratory, Central Laser Facility, Oxfordshire, OX11 0QX, UK*
(Received 10 December 2010; published 10 March 2011)

Experiments were performed using the OMEGA EP laser, operating at 740 J of energy in 8 ps (90 TW), which provides extreme conditions relevant to fast ignition studies. A carbon and hydrogen plasma plume was used as the underdense target and the interaction of the laser pulse propagating and channeling through the plasma was imaged using proton radiography. The early time expansion, channel evolution, filamentation, and self-correction of the channel was measured on a single shot via this method. A channel wall modulation was observed and attributed to surface waves. After around 50 ps, the channel had evolved to show bubblelike structures, which may be due to postsoliton remnants.

The interaction of high-energy (~ 100s J, >50 TW), relativistically intense laser pulses with underdense plasma is of fundamental interest for a number of applications. A plasma is "underdense" and allows the propagation of an electromagnetic wave (wavelength in μm, λ_μ) if the plasma density, n_e, is below the critical density, $n_c = \epsilon_0 m_e \omega_L^2 / e^2 = 1.12 \times 10^{21}/\lambda_\mu^2$ cm^{-3}. Many nonlinear processes can be involved in laser pulse propagation through a plasma, such as ponderomotive and relativistic self-focusing [1,2] leading to channeling [3], filamentation [4,5], scattering [6], hosing [7], and production of solitons [8–10]. Formation of a depleted plasma channel enables ultrarelativistic electron beam acceleration through direct laser acceleration [11]. Oscillations of these electrons in the channel consequently generates synchrotron x rays [12] and electron displacement leads to ion acceleration [13] and blast wave formation [14]. At extreme intensities, complete cavitation of the channel can also be achieved [5].

A potentially important application is the hole boring scheme for fast ignition inertial confinement fusion [15]. A high-energy, short laser pulse has to channel through millimeter-scale underdense plasma to reach a dense fuel core [16]. Modeling on scales relevant to fast ignition has been performed using two-dimensional particle-in-cell (PIC) codes and has previously demonstrated stable channel formation [16]. The laser parameters required for a channeling pulse to reach the critical density were found to be ~ 100 ps at intensities of $I \approx 5 \times 10^{18} – 10^{20}$ W cm^{-2} with an energy of $E_c \approx 1.7(I/10^{18}$ W cm$^{-2})^{0.36}$ kJ ≈ 3–9 kJ [16]. Previous channeling experiments have used optical interferometry [3,5], X-UV radiography [17], x-ray pinhole camera imaging [18], and proton probing [10,19,20]. However, none of these have simultaneously used long-pulse length ($\gg 1$ ps) with high-power (~ 100 TW), which are required for fast ignition experiments [16].

In this Letter, a plasma channel was formed by a 740 J, 8 ps (90 TW) laser pulse focused to a peak vacuum intensity of around 2.8×10^{19} W cm^{-2} into a carbon and hydrogen (CH) plasma plume with a peak density of $n_e = 5 \times 10^{19}$ cm^{-3} ($0.05 n_c$). Proton radiography [21] was used to image the evolution of the electromagnetic fields in the channel formed by the interaction and observed filamentation of the laser, self-correction of the channel, and channel wall modulations. The experimental results are compared to two-dimensional PIC simulations, which show the generation surface waves and subsequent generation in to larger scale modulations.

The experiment was performed at the Laboratory for Laser Energetics using the OMEGA EP laser system. A single long-pulse ($\sim$ nanosecond) laser was used to create an underdense plasma target and two "short-pulse" ($\sim$ picosecond) beams provided the main interaction pulse and a pulse to generate a proton probe beam. A schematic of the experimental configuration is shown in Fig. 1(a). The long pulse had a 2.5 ns super-Gaussian temporal profile at a wavelength of 352 nm (3ω). A laser energy of (1160 ± 110) J was incident at 55° to the target normal and focused to a 800 μm diameter super-Gaussian profile focal spot using distributed phase plates. The intensity on the 150 μm thick planar plastic (CH) target was 1.0×10^{14} W cm^{-2}, which created a plasma plume. The two-dimensional hydrodynamic code SAGE [22] was used to model the heating and expansion of the fully ionized CH plasma plume into the vacuum. Figure 1(b) shows the electron density profile, which was well approximated by a Gaussian function of half-width $= 650 \mu$m with a peak plasma density of $n_e = (5.3 \pm 0.5) \times 10^{19}$ cm$^{-3} = 0.053$ n$_c$, with the error in the peak density due to shot-to-shot fluctuations in laser beam energy. The plasma plume temperature in

(a) experimental set-up

Proton probe pulse

Cu foil

proton beam

Main interaction pulse (743 J, 8.2 ps)

RCF detector stack

UV Long-pulse (1160 J, 2.5 ns)

CH foil & plasma plume

(b) density profile

n_e (10^{19} cm^{-3})

radius (mm)

(c) focal spot data

Peak Intensity [10^{19} Wcm^{-2}]

Peak a_0

x (µm)

y (µm)

y (µm)
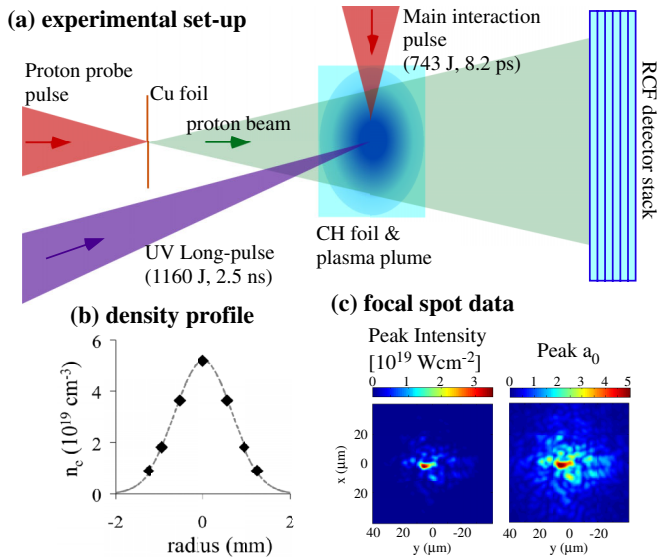
FIG. 1 (color online). (a) Schematic of the experimental configuration for the proton radiography of the underdense plasma interaction. (b) The plasma density profile of the main interaction pulse path from SAGE, with Gaussian fit. (c) Typical focal spot data showing the calculated peak intensity and the peak a_0 for the main interaction pulse.

focus ↓ peak n_e

$t_0 + 11.5$ ps

$t_0 + 18.8$ ps

1mm

$t_0 + 14.7$ ps

focus

peak n_e

filamentation

dark region

channel

$t_0 + 18.8$ ps

$t_0 + 22.6$ ps

channel self-correction

$t_0 + 27.6$ ps

channel wall modulations

(zoom x 3)

$t_0 + 33.6$ ps

100µm

500 µm

FIG. 2 (color online). Sequence of proton probe images (left), with a blowup of one image (right). The inset shows a region of the channel wall. The laser pulse was traveling from left to right.

this region is 200–300 eV so the assumption of full ionization is reasonable.

The main interaction pulse had an on-target energy of $E_L = (743 \pm 11)$ J with a full-width half-maximum (FWHM) pulse length of $\tau_L = (8.2 \pm 0.4)$ ps giving an average pulse power of approximately 90 TW. The linearly polarized laser had a central wavelength of 1.053 µm. An $f/2$ off-axis parabolic mirror focused the pulse to 0.8 mm before the center of the plume, where $n_e = 2.5 \times 10^{19}$ cm$^{-3} = 0.025$ n_c. If a laser pulse exceeds a critical power, $P_c \approx 17.5(n_c/n_e)$ GW, relativistic self-focusing will overcome diffraction and the pulse will be guided [1]. Here, $P_c \approx 0.7$ TW and therefore was well into the relativistic self-focusing regime. Ponderomotive self-focusing will also contribute as the channel is formed. Assuming a Gaussian temporal profile, the peak vacuum intensity for the presented shots was $(2.8 \pm 0.7) \times 10^{19}$ Wcm^{-2}, corresponding to peak normalized vector potential of $a_0 = (4.7 \pm 0.6)$. Typical peak intensity and a_0 maps are given in Fig. 1(c), which were reconstructed using measured wave front data [23]. For creating the proton radiography beam, a pulse with either $E_L \approx 230$ J and $\tau_L = 1$ ps (or $E_L \approx 930$ J and $\tau_L = 9$ ps for some of the Fig. 3 shots) were focused onto a 50 µm thick copper foil. There was an error of ± 10 ps on the given timing due to jitter between the laser pulses. A proton beam originating from the rear side of the target was generated through target normal sheath acceleration [24]. The protons were detected on a radiochromic film pack and since the time required for the protons to travel from the source foil to the interaction depends on the proton energy,

different film layers imaged different times in the interaction to create an image sequence. The image magnification is between 15–18 (depending on the radiochromic film layer) with a spatial resolution of ~20 µm.

The proton images in Fig. 2 show the plasma interaction during the formation of the channel. The time at which the leading edge of the pulse arrived at focus and reached half-maximum intensity (4.1 ps before the peak intensity) was defined as t_0. The relative timing between the images is known to a high accuracy from the proton energies. The channel expelled protons from the central region due to the quasistatic electromagnetic fields. The channel broke up into a number of filaments, suggesting that the laser had also split into several individual filaments. As the interaction progressed, the ends of the filaments merge [as shown in the Fig. 2 time sequence] at a speed of $\approx 0.1c$ and eventually self-corrected into a single channel. A dark region in the center of the channel appeared after the initial stages of channel formation and progressed through the channel at a speed of $\approx 0.12c$, which likely indicates a region of field inversion inside the channel [20]. The inset to the large image shows channel wall modulations with a scale of ≈ 50 µm.

The evolution of the channel over a longer time scale is illustrated in Fig. 3, which shows data from a number of shots taken with different relative short-pulse beam timing. After a time of approximately $t_0 + 40$ ps, bubblelike structures start to develop along the filaments and over time they grow larger in size. The structures are not so prevalent at the beginning of the channel. The channel has expanded to a diameter of 500–800 µm by $t_0 + 187$ ps. The protons have been deflected from the bubblelike regions, which indicates the structures must have associated quasistatic electromagnetic fields. The typical size of the structures was in the range 50–200 µm. Similar late time *density* instabilities have previously been observed in blast wave
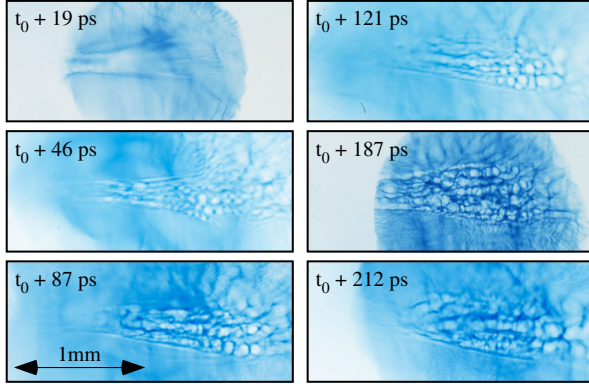
FIG. 3 (color online).   Proton probe image sequence showing the temporal evolution of the channel based on different shots. The laser propagation was from left to right.

structures [14] and were attributed to the Dyakov-Kontorovich instability [25].

To model the interaction, 2D3P PIC simulations were performed using the OSIRIS 2.0 code [26]. The simulation box is 2 mm × 1 mm with a resolution of 12.6 cells/λ in the longitudinal (x) direction and 3 cells/λ in the transverse direction (y) and 16 particles per cell. The proton plasma had a density profile which was Gaussian with a half-width of 500 μm in the x direction and had an exponential gradient in the y direction, to mimic the experiment. The maximum density along the laser propagation axis was $0.05n_c$. The laser pulse was linearly polarized with the electric field in the y direction, with a FWHM $\tau_L = 8$ ps and $\lambda = 1.053$ μm. The peak of the pulse entered the simulation box at 10.4 ps. To approximate the experimental energy distribution in the focal plane [Fig. 1(c)], two overlapped pulses were used, one for the central hotspot focused to $w_0 = 3.4$ μm with $a_0 \approx 5.5$ and the other to simulate the wider energy distribution, focused to $w_0 = 16$ μm with $a_0 \approx 1.5$. The focal plane was 800 μm before the peak density.

Figure 4 presents electron density data from the simulation. The laser envelope at $t = 9$ ps has filamented, creating a number of channels in the electron density [Fig. 4(a)] containing high-energy electron currents. These accelerated electrons travel along the center of the channel, with return currents running along the walls of the channel. The laser continues to exert ponderomotive pressure on the channel walls and the individual channels merge into a single channel structure. The walls of the channel at 11 ps display modulation [Fig. 4(b)], having a wavelength of ≈ 15–20 μm, which is likely due to surface wave excitation [7,27]. If the laser pulse undergoes a hosing instability, intensity modulations can be created and surface wave modulations can be excited [7]. In the simulation, hosing was observed, which created intensity modulations in the laser envelope [Fig. 5(c)]. The surface wave frequency is $\omega_{sw} \approx \omega_p^2/\omega_L$, and providing the
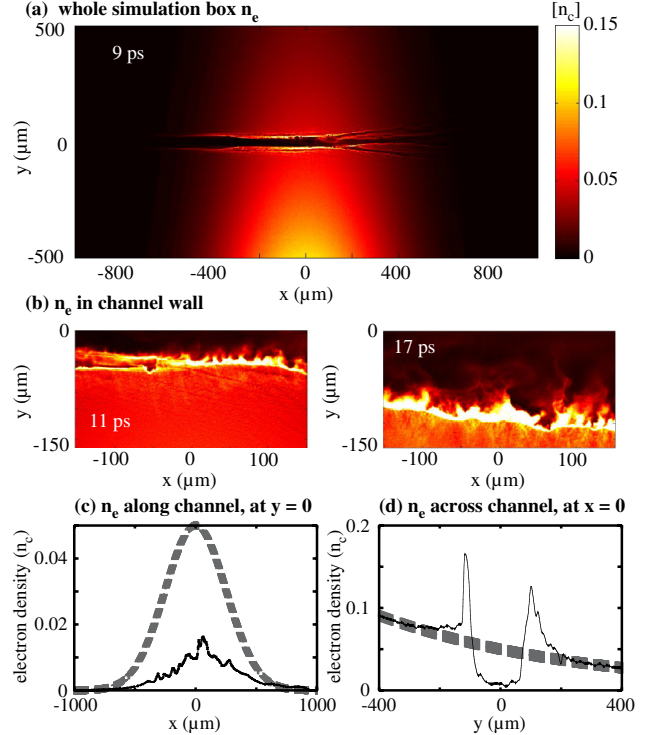
FIG. 4 (color online).   Electron density, n_e, data from the 2D simulations showing (a) the whole simulation box with the filamented channels, (b) the channel wall modulations at times of 11 ps and 17 ps. (c),(d) Lineouts along the center and across the channel at peak density initially (dashed) and at 13.5 ps (solid).

channel width is much greater than the electron skin depth c/ω_p, where ω_L is the laser frequency [7]. This gives a wavelength of $\approx 21\mu$m for $n_e = 0.05n_c$. The laser can also interact with the channel walls to drive surface wakes [27,28]. Generation of electron density modulations and acceleration through surface modes may be responsible for the injection of fast electrons back into the laser fields within the cavitated channel, enabling direct laser acceleration of electrons [27]. After a few more picoseconds, the modulation relaxed into a longer wavelength [≈ 40 μm, shown in Fig. 4(b)], which was in reasonable agreement with the experimental observations. Along the center of the channel the plasma density peaked at $0.015n_c$, or $\approx 30\%$ of the initial density [Figs. 4(c) and 4(d)].

Both the magnetic fields in the z direction, associated with the electron currents [Fig. 5(b)] and the y-direction electric fields [Fig. 5(a)] show complex field structures, particularly near where the filaments collide. Ahead of the visible channel formation, strong transverse electric fields with a rippled structure have formed, which are very similar to structures observed in the proton images. Transverse electric field inversion occurred as the radially accelerated ions reach the electron walls. This affected the laser propagation by allowing laser energy to "leak" through the channel walls [29].
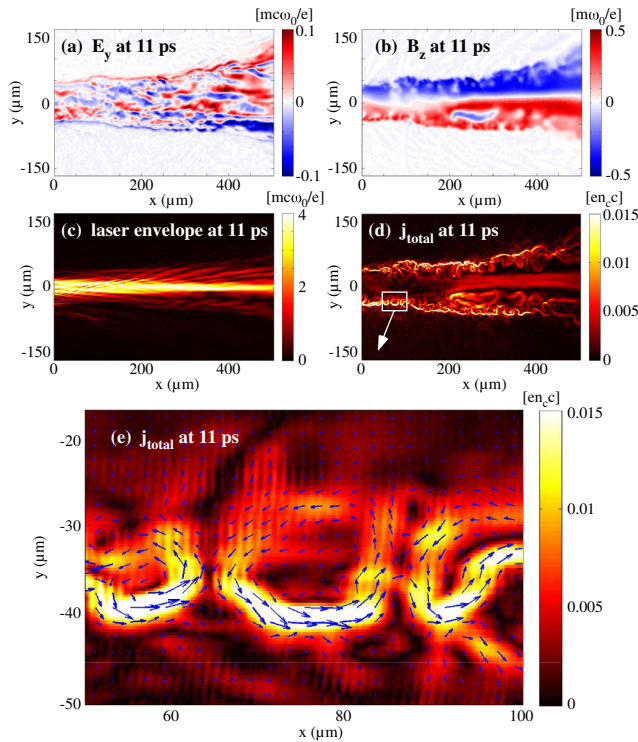
FIG. 5 (color online). (a) The y-direction electric field, E_y, (b) the z-direction magnetic field, B_z, (c) the laser envelope, and (d) the total current density at 11 ps. Panel (e) is an enlarged region showing the total currents and flow vectors.

As the channel evolved, current loops developed near the walls of the channel and expanded with time [Figs. 5(d) and 5(e)], the return current ran along the outer region of the channel wall. Simulations have identified soliton production [8] and post-soliton remnants [29], which were recently observed experimentally [10].

In conclusion, proton probing was used to image the interaction of a high-energy, high-power laser pulse through a millimeter-scale plasma with a peak density of $0.05 n_c$ The experiment and simulations both show that the laser underwent filamentation leading to the formation of a number of individual channels. The ponderomotive pressure of the laser corrected the channel into a single hollow structure, which had a low residual plasma density making it suitable to efficiently transmit an ignition pulse. Modulations in the wall of the channel were observed and were likely seeded by surface wave excitation. At later times, the proton probe observed bubblelike structures, which may be associated with postsoliton remnants. There was minimal density perturbations associated with these structures within the channel so they should not significantly impede the transmission of laser light, although the mode structure might change.

[1] P. Sprangle, C.-M. Tang, and E. Esarey, IEEE Trans. Plasma Sci. **15** 145 (1987).
[2] A. B. Borisov *et al.*, Phys. Rev. Lett. **65**, 1753 (1990).
[3] M. Borghesi *et al.*, Phys. Rev. Lett. **78**, 879 (1997).
[4] Z. Najmudin *et al.*, Phys. Plasmas **10**, 438 (2003)
[5] P. M. Nilson *et al.*, New J. Phys. **12**, 045014 (2010).
[6] D. W. Forslund, J. M. Kindel, and E. L. Lindman, Phys. Fluids **18**, 1002 (1975).
[7] N. M. Naumova *et al.*, Phys. Plasmas **8**, 4149 (2001).
[8] N. M. Naumova *et al.*, Phys. Rev. Lett. **87**, 185004 (2001); T. Esirkepov *et al.*, *ibid.* **89**, 275002 (2002); T. Esirkepov *et al.*, *ibid.* **92**, 255001 (2004).
[9] M. Borghesi *et al.*, Phys. Rev. Lett. **88**, 135002 (2002).
[10] L. Romagnani *et al.*, Phys. Rev. Lett. **105**, 175002 (2010).
[11] S. P. D. Mangles *et al.*, Phys. Rev. Lett. **94**, 245001 (2005).
[12] S. Kneip *et al.*, Phys. Rev. Lett. **100**, 105006 (2008).
[13] N. H. Burnett and G. D. Enright, IEEE J. Quantum Electron. **26**, 1797 (1990); K. Krushelnick *et al.*, Phys. Rev. Lett. **83**, 737 (1999); M.-S. Wei *et al.*, Phys. Rev. Lett. **93**, 155003 (2004); L. Willingale *et al.*, Phys. Rev. Lett. **96**, 245002 (2006).
[14] P. M. Nilson *et al.*, Phys. Rev. Lett. **103**, 255001 (2009).
[15] M. Tabak *et al.*, Phys. Plasmas **1**, 1626 (1994).
[16] G. Li *et al.*, Phys. Rev. Lett. **100**, 125002 (2008).
[17] K. Takahashi *et al.*, Phys. Rev. Lett. **84**, 2405 (2000).
[18] A. L. Lei *et al.*, Phys. Rev. E **76**, 066403 (2007).
[19] G. Sarri *et al.*, Phys. Plasmas **17**, 113303 (2010).
[20] S. Kar *et al.*, New J. Phys. **9**, 402 (2007)
[21] M. Borghesi *et al.*, Rev. Sci. Instrum. **74**, 1688 (2003).
[22] R. S. Craxton and R. L. McCrory, J. Appl. Phys. **56**, 108 (1984).
[23] J. Bromage *et al.*, Opt. Express **16**, 16561 (2008).
[24] S. P. Hatchett *et al.*, Phys. Plasmas **7**, 2076 (2000).
[25] S. P. Diakov, J. Exp. Theor. Phys. **27**, 288 (1954); V. M. Kontorovich, *ibid.* **33**, 1525 (1957); V. M. Kontorovich, Akust. Zh. **5**, 314 (1959).
[26] R. O. Fonseca *et al.*, *Lecture Notes in Computer Science* (Springer, Heidelberg, 2002), Vol. 2329, pp. III-342.
[27] N. Naseri *et al.*, Phys. Plasmas **17**, 033107 (2010).
[28] T. C. Chiou *et al.*, Phys. Plasmas **2**, 310 (1995).
[29] A. Macchi *et al.*, Plasma Phys. Controlled Fusion **49**, B71 (2007).